Further insights into controlling anisotropy of pentacoordinate Co(II) field-supported single-molecule magnets.

Katarzyna Choroba[a], Barbara Machura*[a], Alina Bieńko*[b], Jacek Sawka[b], Dariusz C. Bieńko[c], Cyril Rajnák[d], Ján Titiš[d], Roman Boča[e] , Mykhaylo Ozerov[f] and Andrew Ozarowski[f]

[a] *Department of Crystallography, Institute of Chemistry, University of Silesia, 9th Szkolna St., 40-006 Katowice, Poland*
[b] *Faculty of Chemistry, University of Wroclaw, Joliot-Curie 14, 50-383 Wroclaw,Poland*
[c] *Faculty of Chemistry, Wroclaw University of Technology, Wybrzeze Wyspiańskiego 27, 50-370 Wroclaw, Poland*
[d] *Faculty of Natural Sciences, University of SS Cyril and Methodius, 91701 Trnava, Slovakia*
[e] *Faculty of Health Sciences, University of SS Cyril and Methodius, 91701 Trnava,Slovakia*
[f] *National High Magnetic Field Laboratory, Florida State University, 1800 East Paul Dirac, Tallahassee, Florida 32310, United States*

ELECTRONIC SUPPLEMENTARY INFORMATION (ESI)

ELECTRONIC SUPPLEMENTARY INFORMATION (ESI)

Table S1. Magneto-structural properties of previously reported mononuclear five-coordinate [Co(R-terpy)X_2] complexes with 2,2′:6′,2″-terpyridine and their 4′-subsitiuted derivatives. A more comprehensive literature survey on magneto-structural properties of five-coordinate Co(II) complexes with tridentate N-donor ligands was given in references [2, 4, 5].

R-terpy	X	τ	EPR	D/cm^{-1} E or E/D	Magnetic properties	Ref.
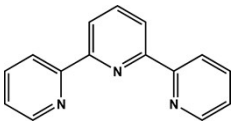	Cl^-	0.05		D = 200 cm^{-1}	$\tau_0 = 1.07\cdot10^{-6}$ s U_{eff} = 19.5 cm^{-1} $\tau_0 = 7.44\cdot10^{-2}$ s U_{eff} = 2.78 cm^{-1}	1
	NCS^-	0.43		D = 100 cm^{-1}	$\tau_0 = 5.85\cdot10^{-6}$ s U_{eff} = 11.8 cm^{-1} τ_0 = 0.11s U_{eff} = 2.1 cm^{-1}	1
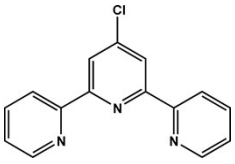	Cl^-	0.07	g_x = 2.49 g_y = 2.49 g_z = 2.86	D = −55.27 cm^{-1} E = 16.19 cm^{-1}	$\tau_0 = 6.3\cdot10^{-2}$ s U_{eff} = 18.8 cm^{-1}	2
	Br^-	0.06	g_x = 2.42 g_y = 2.42 g_z = 2.76	D = −48.71 cm^{-1} E = 15.38 cm^{-1}	—	2
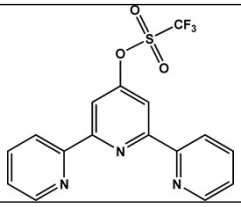	Cl^-	0.23	$g_{\parallel}$ = 2.26 $g_{\perp}$ = 2.98	D = –22.2 cm^{-1} E = 3.53 cm^{-1}	—	3

1) Habib, F.; Luca, O. R.; Vieru, V.; Shiddiq, M.; Korobkov, I.; Gorelsky, S. I.; Takase, M. K.; Chibotaru, L. F.; Hill, S.; Crabtree, R. H.; Murugesu, M. Influence of the Ligand Field on Slow Magnetization Relaxation versus Spin Crossover in Mononuclear Cobalt Complexes. *Angewandte Chemie International Edition* 2013, **52** (43), 11290–11293. https://doi.org/10.1002/anie.201303005.

2) Slavensky, H.H; Parmar, V.S; Leiszner, S.S; Thiel, A.M.; Lassen,H.; Calder, S; Kibalin, I.; Iversen, B.B. Experimental determination of the magnetic anisotropy in five-coordinated Co(II) field-induced single molecule magnets. Chem. Sci., 2025, **16**, 16610. https:// doi: 10.1039/d5sc03103f.

3) Higgins, R. F.; Livesay, B. N.; Ozumerzifon, T. J.; Joyce, J. P.; Rappé, A. K.; Shores, M. P. A Family of Related Co(II) Terpyridine Compounds Exhibiting Field Induced Single-Molecule Magnet Properties. *Polyhedron*, 2018, ***143***, 193–200. https://doi.org/10.1016/j.poly.2017.10.008.

4) Choroba. K.; Palion-Gazda, J.; Machura, B.; Bieńko, A.; Wojtala, D.; Bieńko, D.; Rajnak, C.; Boča, R.; Ozarowski, A.; Ozerov M. Large Magnetic Anisotropy in Mono- and Binuclear

cobalt(II) Complexes: The Role of the Distortion of the Coordination Sphere in Validity of the Spin-Hamiltonian Formalism *Inorg. Chem.* 2024, **63**, 1068−1082. https://doi.org/10.1021/acs.inorgchem.3c03405.

5) Juráková, J.; and Salitros, I. Co(II) single-ion magnets: synthesis, structure, and magnetic properties, *Monatsh Chem*, 2022, **153**, 1001-1036. https://doi.org/10.1007/s00706-022-02920-0

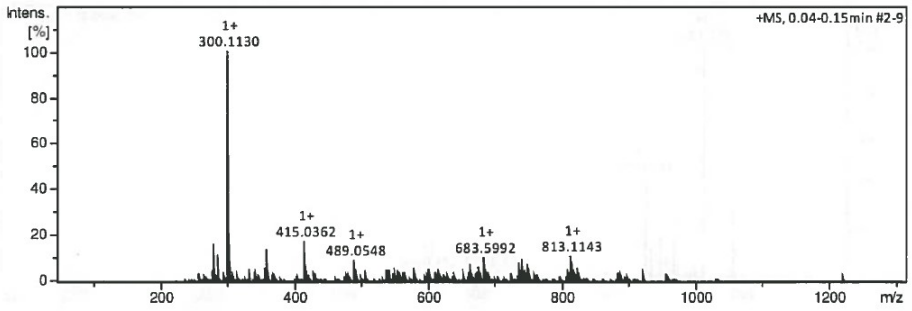

Meas. m/z	#	Ion Formula	Score	m/z	err [mDa]	err [ppm]	mSigma	rdb	e— Conf	N-Rule	Adduct
300.1130	1	C19H14N3O	100.00	300.1131	-0.1	-0.4	4.1	14.5	even	ok	M+H

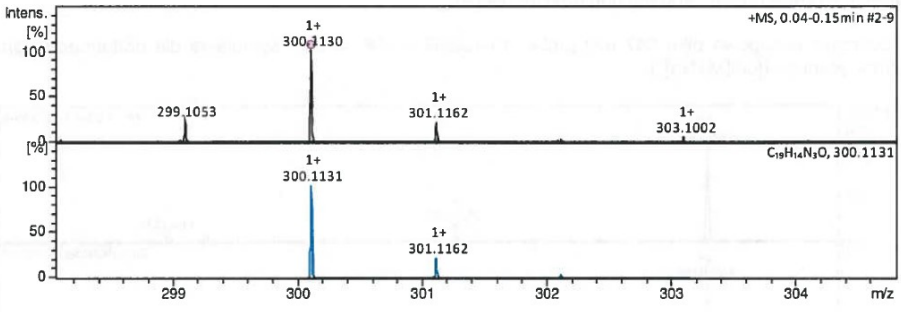

1

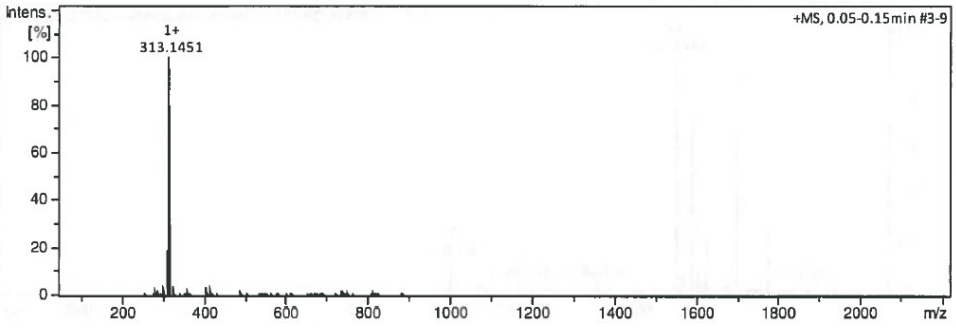

Meas. m/z	#	Ion Formula	Score	m/z	err [mDa]	err [ppm]	mSigma	rdb	e— Conf	N-Rule	Adduct
313.1451	1	C20H17N4	100.00	313.1448	0.3	1.1	25.9	14.5	even	ok	M+H

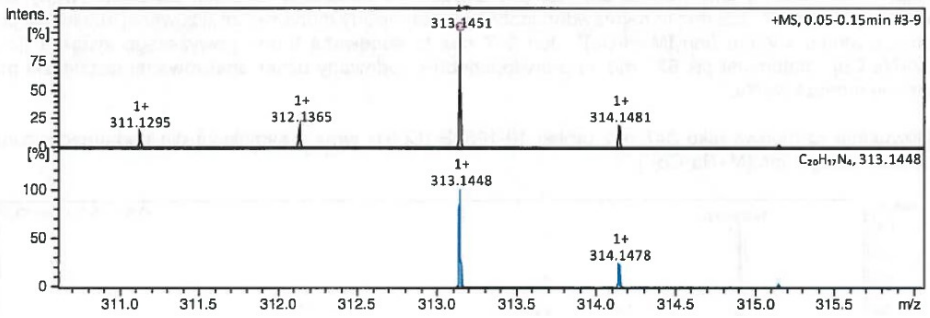

2

Figure S1. HR-APCI-MS spectra of compounds **1** and **2**

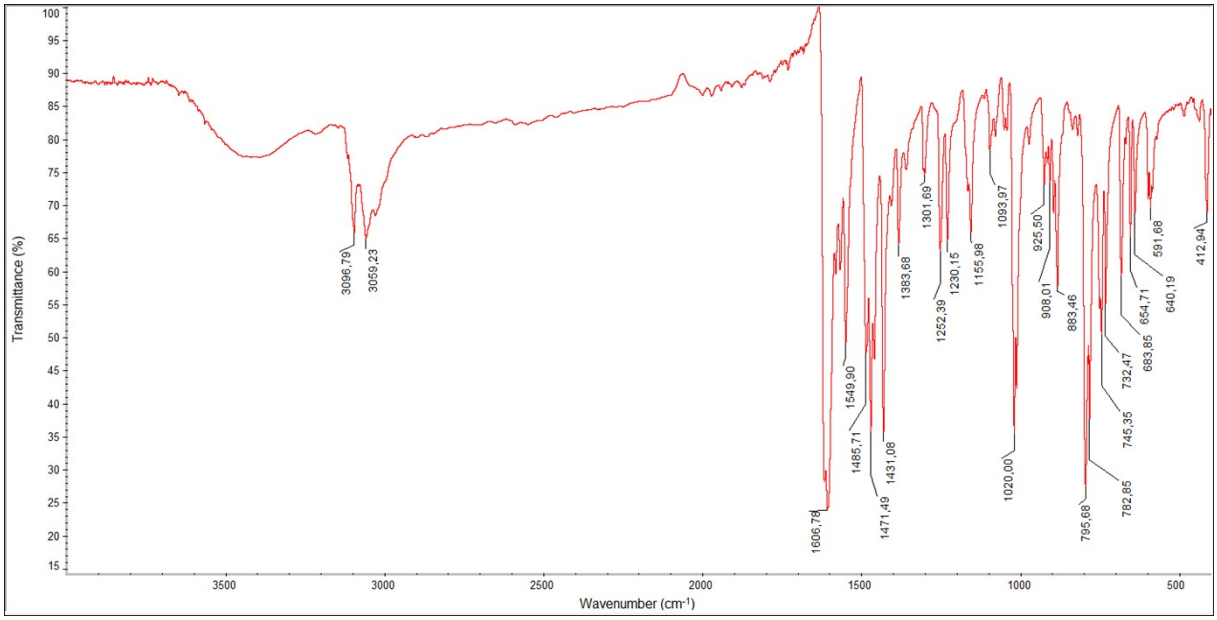

1

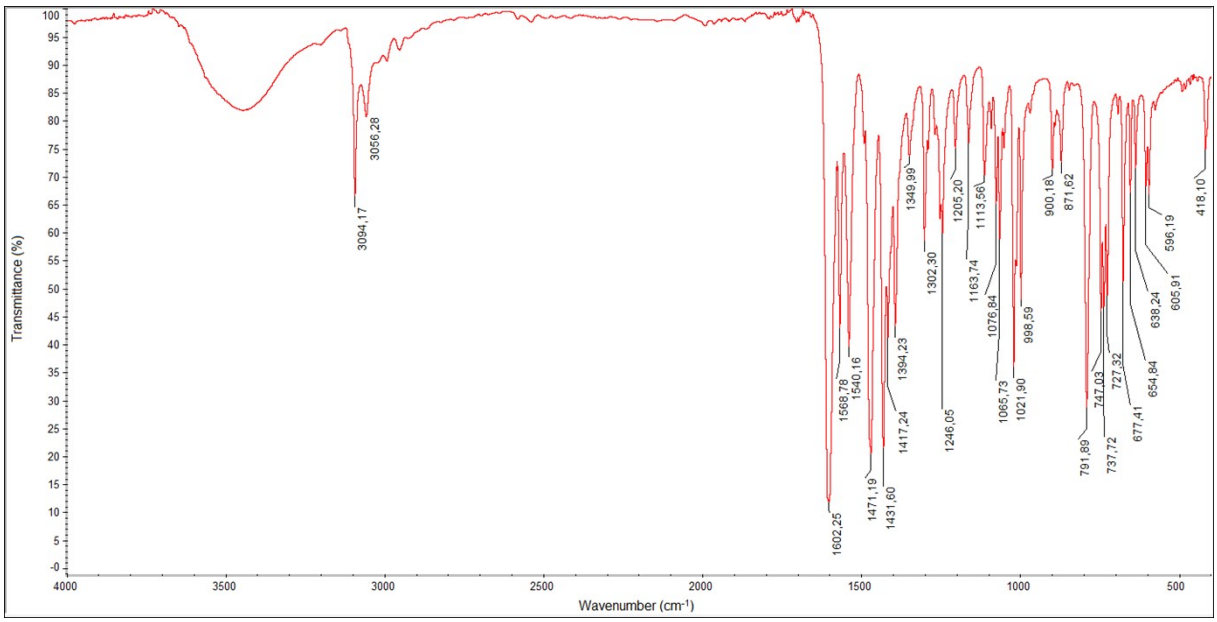

2

Figure S2a. IR spectra of compounds **1-2**.

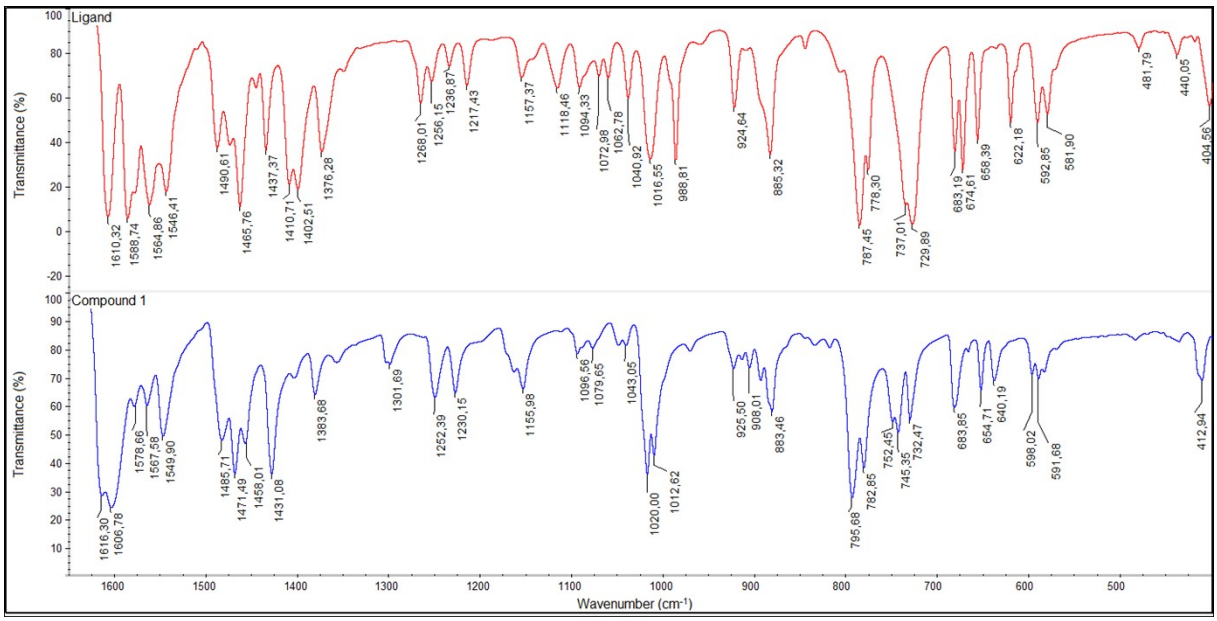

1

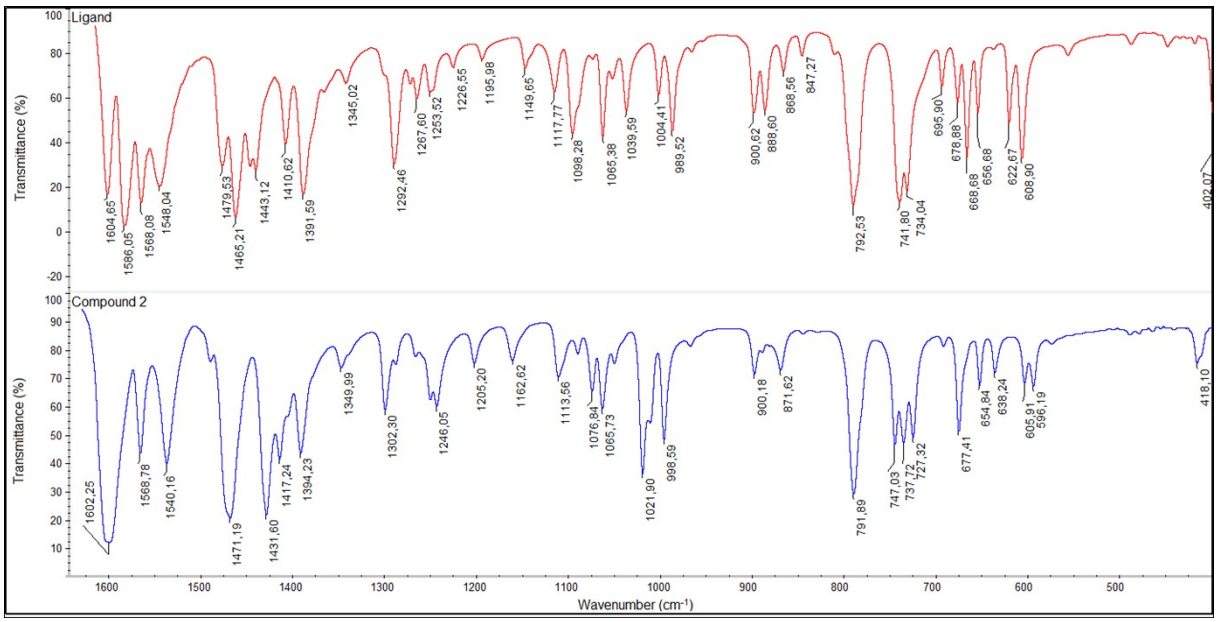

2

Figure S2b. IR spectra of compounds **1-2** (blue) compared with IR spectrum of the free ligand (red).

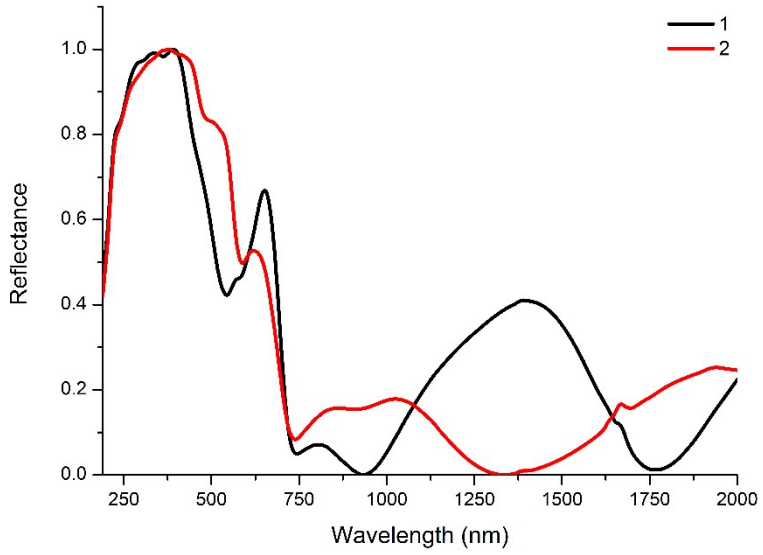

Figure S3. UV-Vis reflectance spectra of compounds **1** and **2.**

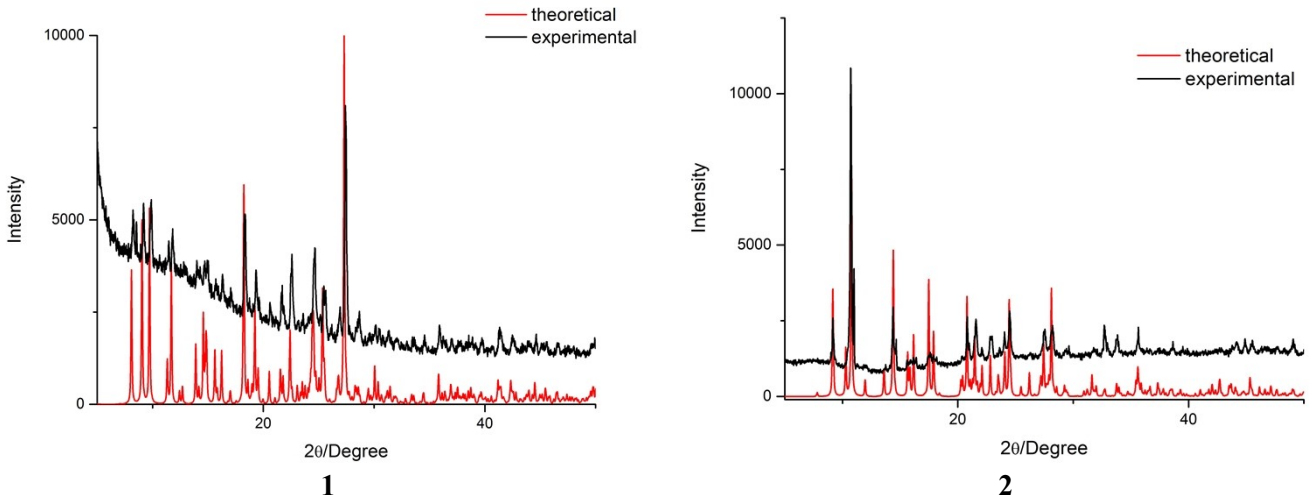

Figure S4. XPRD patterns of compounds **1** and **2**.

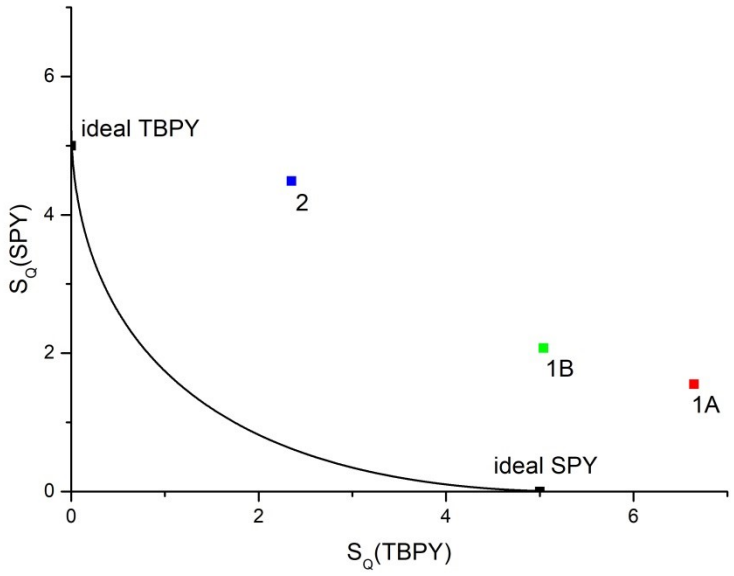

Figure S5. Berry pseudorotation minimum distortion path and the deviations of **1A-B** and **2** from the path. Significant deviation of the experimental geometries from the Berry pseudorotation path in the shape map of the minimum distortion interconversion path SPY/TBY is attributed to the constraints imposed by the chelate ligand and inequality in bond distances)

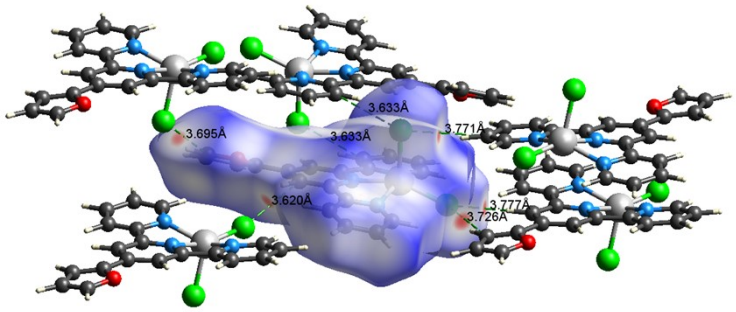

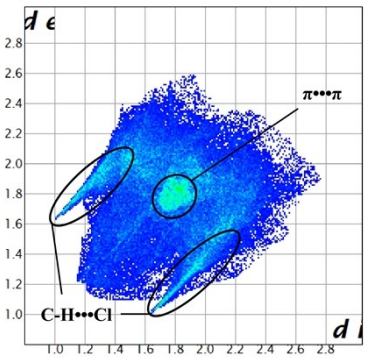

1A

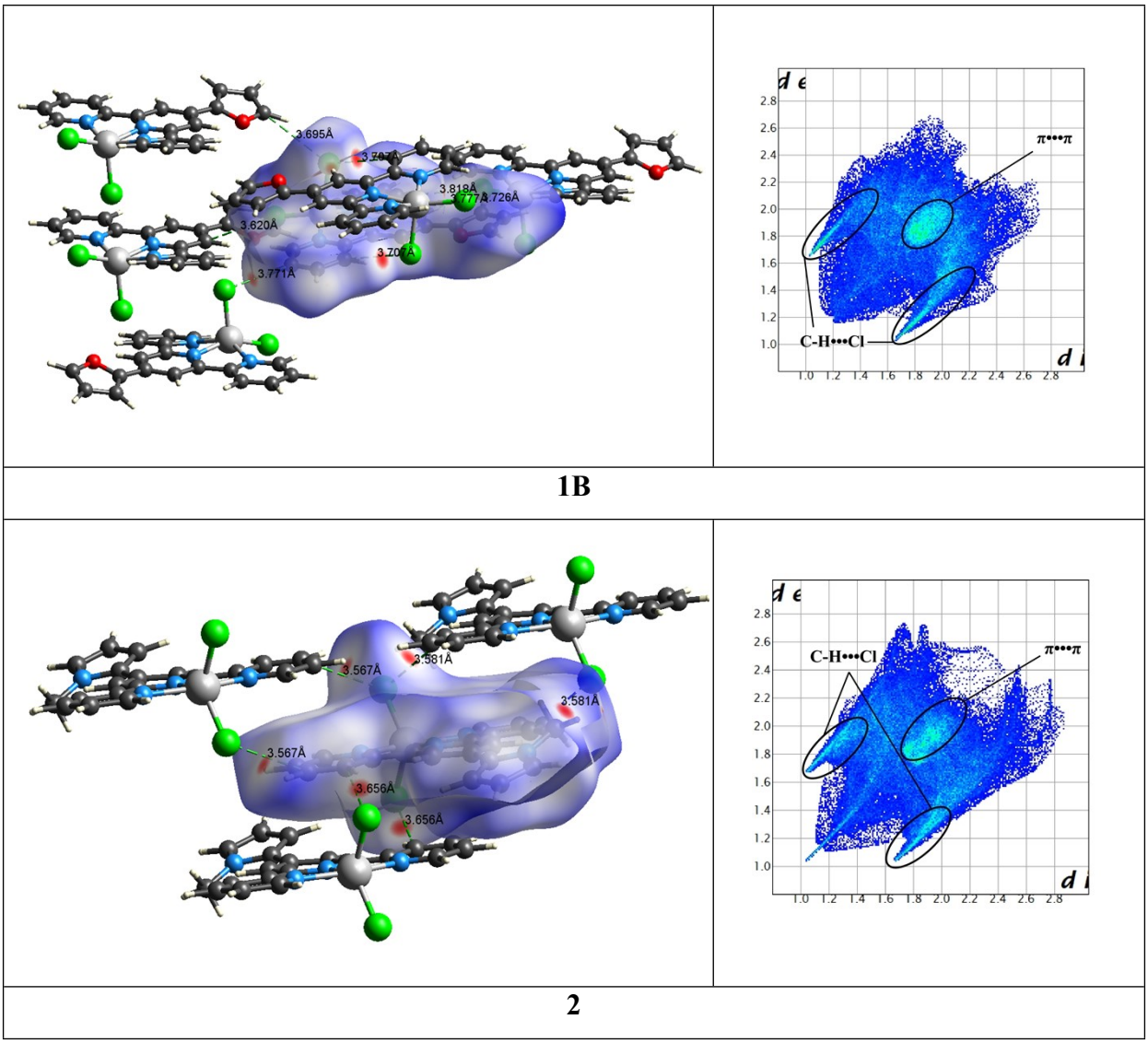

Figure S6. Hirshfeld surface mapped with d_{norm} (a) and 2D fingerprint plots (b) for **1A-B** and **2**.

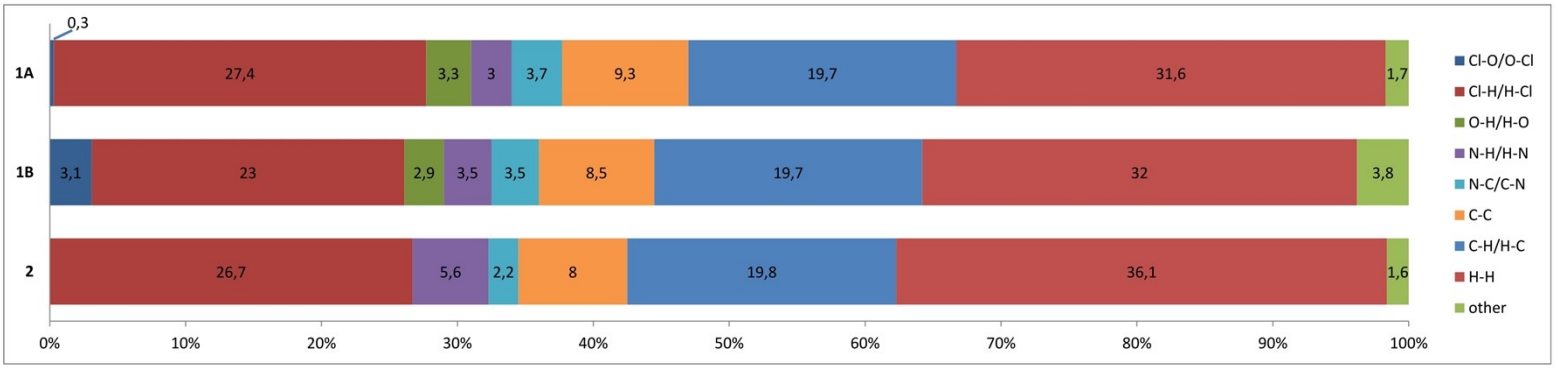

Figure S7. Relative contributions of various intermolecular interactions to the Hirshfeld surfaces for **1A-B** and **2**.

Table S2. The selected bond lengths [Å] and anges [°] of compounds **1** and **2**.

Bond lengths [Å]			
		1	**2**
Co(1)–N(1)	molecule A	2.143(2)	2.160(2)
Co(1)–N(2)		2.0599(19)	2.037(2)
Co(1)–N(3)		2.149(2)	2.157(2)
Co(1)–Cl(1)		2.2735(7)	2.2779(9)
Co(1)–Cl(2)		2.3093(8)	2.2831(8)
Co(2)–N(4)	molecule B	2.128(2)	
Co(2)–N(5)		2.0719(18)	
Co(2)–N(6)		2.130(2)	
Co(2)–Cl(3)		2.2801(7)	
Co(2)–Cl(4)		2.3296(8)	
Bond angles [°]			
		1	**2**
N(1)–Co(1)–N(2)	molecule A	75.08(7)	76.18(8)
N(2)–Co(1)–N(3)		74.98(8)	76.42(8)
N(1)–Co(1)–N(3)		143.05(8)	152.59(8)
Cl(1)–Co(1)–N(1)		98.36(6)	95.16(6)
Cl(1)–Co(1)–N(2)		152.51(6)	122.95(6)
Cl(1)–Co(1)–N(3)		98.25(6)	99.15(7)
Cl(2)–Co(1)–N(1)		102.74(6)	97.32(6)
Cl(2)–Co(1)–N(2)		95.33(6)	123.64(6)
Cl(2)–Co(1)–N(3)		101.13(6)	98.26(6)
Cl(1)–Co(1)–Cl(2)		112.16(3)	113.35(3)
C(1)–N(1)–C(5)		118.5(2)	118.3(2)
C(6)–N(2)–C(10)		120.5(2)	119.2(2)
C(11)–N(3)–C(15)		118.5(2)	118.1(2)
N(4)–Co(2)–N(5)	molecule B	74.70(7)	
N(5)–Co(2)–N(6)		74.34(8)	
N(4)–Co(2)–N(6)		139.87(8)	
Cl(3)–Co(2)–N(4)		99.46(6)	
Cl(3)–Co(2)–N(5)		162.69(7)	
Cl(3)–Co(2)–N(6)		102.55(6)	
Cl(4)–Co(2)–N(4)		106.05(6)	
Cl(4)–Co(2)–N(5)		90.86(6)	
Cl(4)–Co(2)–N(6)		99.32(6)	
Cl(3)–Co(2)–Cl(4)		106.44(3)	
C(20)–N(4)–C(24)		118.9(2)	
C(25)–N(5)–C(29)		121.2(2)	
C(30–N(6)–C(34)		118.1(2)	

Table S3. Short intra- and intermolecular hydrogen bonds detected in cobalt compounds.

D–H•••A	D–H [Å]	H•••A [Å]	D–A [Å]	D–H•••A [°]
1				
C(4)–H(4)•••Cl(2)[a]	0.93	2.76	3.633(3)	156.3
C(9)–H(9)•••Cl(3)[b]	0.93	2.82	3.620(3)	145.4
C(23)–H(23)•••Cl(4)[c]	0.93	2.81	3.707(3)	163.3
C(36)–H(36)•••Cl(1)	0.93	2.82	3.725(3)	165.4
2				
C(3)–H(3)•••Cl(2)[d]	0.93	2.81	3.567(3)	138.8
C(4)–H(4)•••Cl(1)[e]	0.93	2.82	3.656(3)	150.4
C(12)–H(12)•••Cl(2)[f]	0.93	2.81	3.582(3)	140.9

Table S4. Short π•••π interactions for cobalt compounds.

Cg(I)•••Cg(J)	Cg(I)•••Cg(J) [Å]	α [°]	β [°]	γ [°]	Cg(I)-Perp [Å]	Cg(J)-Perp [Å]
1						
Cg(1)•••Cg(2)[a]	3.9074(16)	1.44(13)	30.41	31.28	-3.3393(11)	-3.3699(11)
Cg(1)•••Cg(2)[g]	3.7107(16)	1.44(13)	21.23	21.69	3.4481(11)	3.4588(11)
Cg(3)•••Cg(3)[h]	3.8473(15)	0	30.10	30.10	-3.3285(11)	-3.3285(11)
Cg(4)•••Cg(5)[c]	3.9310(18)	7.53(17)	26.74	32.87	3.3015(14)	3.5106(11)
Cg(5)•••Cg(6)[i]	3.9768(15)	5.51(12)	26.25	31.59	-3.3874(11)	-3.5667(9)
2						
Cg(1)•••Cg(1)[d]	3.8834(17)	0	28.06	28.06	3.4270(11)	3.4271(11)
Cg(1)•••Cg(2)[e]	3.7130(16)	3.49(13)	25.89	22.45	-3.4316(11)	-3.3402(11)
Cg(2)•••Cg(3)[j]	3.9795(17)	3.24(14)	22.10	21.20	3.7103(11)	3.6870(13)

α = dihedral angle between *Cg*(I) and *Cg*(J); *Cg*(I)-Perp = Perpendicular distance of *Cg*(I) on ring J; *Cg*(J)-Perp = perpendicular distance of *Cg*(J) on ring I; β = angle *Cg*(I)→*Cg*(J) vector and normal to ring I; γ = angle *Cg*(I) →*Cg*(J) vector and normal to plane J;

Table S5. X—Y•••Cg(J)(π-ring) interactions for cobalt compounds.

Y-X(I)•••Cg(J)	X(I)•••Cg(J) [Å]	X-Perp [Å]	γ [°]	Y-X(I)•••Cg(J) [°]
1				
no X—Y•••Cg(J) interactions detected for **1**				
2				
Co(1)-Cl(1)•••Cg(7)[k]	3.7021(17)	3.478	20.03	146.90(4)

γ = angle X(I)→Cg(J) vector and normal to plane J.

Cg1 is the centroid of atoms N(1)/C(1)/C(2)/C(3)/C(4)/C(5); Cg2 is the centroid of atoms N(2)/C(6)/C(7)/C(8)/C(9)/C(10); Cg3 is the centroid of atoms N(3)/C(11)/C(12)/C(13)/C(14)/C(15); Cg4 is the centroid of atoms O(2)/C(35)/C(36)/C(37)/C(38); Cg5 is the centroid of atoms N(4)/C(20)/C(21)/C(22)/C(23)/C(24); Cg6 is the centroid of atoms N(5)/C(25)/C(26)/C(27)/C(28)/C(29); Cg7 is the centroid of atoms N(4)/C(16)/C(17)/C(18)/C(19);

Symmetry codes: (a) = -*x*,1-*y*,-1-*z*; (b) = *x*,*y*,-1+*z*; (c) = 2-*x*,-*y*,-*z*; (d) = 1-*x*,1-*y*,-*z*; (e) = -*x*,1-*y*,-*z;* (f) = 1-*x*,1-*y*,1-*z;* (g) = 1-*x*,1-*y*,-1-*z*; (h) = 1-*x*,-*y*,-1-*z*; (i) = 1-*x*,-*y*,-*z*; (j) = -*x*,1-*y*,1-*z;* (k) = *x*,-1+*y*,*z*.

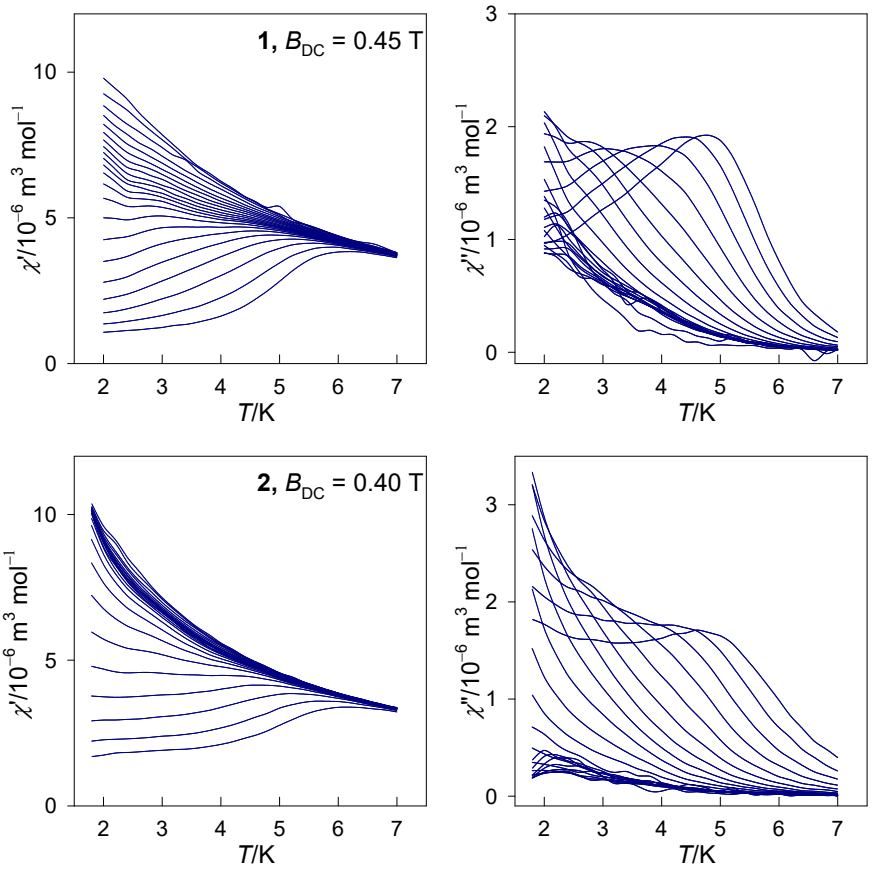

Figure S8. Temperature dependence of the AC susceptibility for **1** and **2** at applied B_{DC} for a set of frequencies f = 0.1 – 1500 Hz.

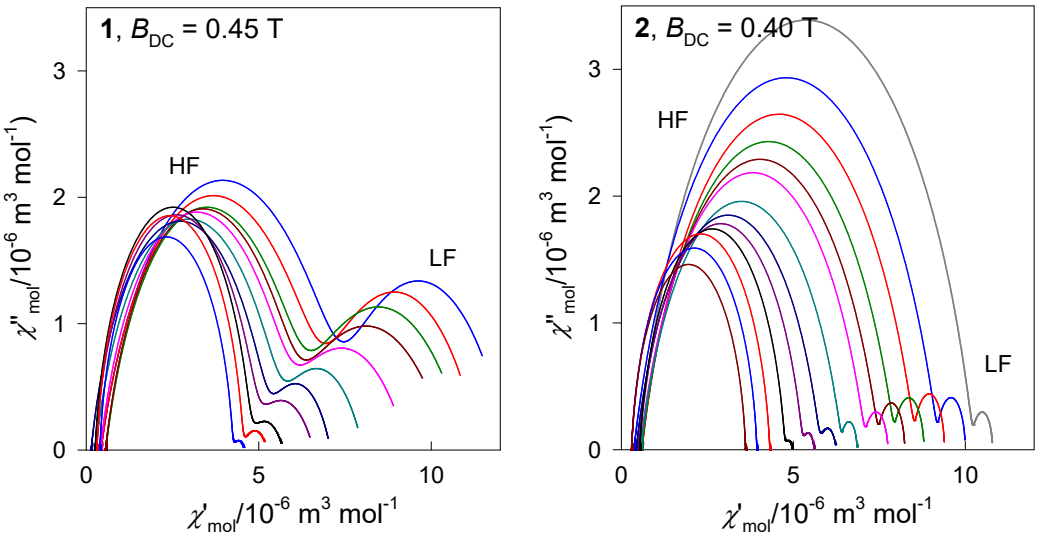

Figure S9. Argand diagram for **1** and **2**.

Table S6. Temperature dependence of AC susceptibility parameters for **1** at B_{DC} = 0.45 T.

T/K	$R(\chi')$ /%	$R(\chi'')$ /%	χ_S	χ_{LF}	α_{LF}	τ_{LF} / s	χ_{HF}	α_{HF}	τ_{HF} /10^{-3} s	x_{LF}	x_{HF}
2.0	0.42	2.2	0.42(4)	5.4(3)	.38(3)	1.5(2)	12.2(2)	.31(1)	1.3(1)	.42	.58
2.2	0.49	1.8	0.43(4)	5.1(2)	.39(2)	1.0(1)	11.4(2)	.29(1)	1.0(1)	.43	.57
2.4	1.0	4.3	0.55(6)	5.5(6)	.46(4)	0.94(21)	11.0(4)	.25(1)	0.79(3)	.47	.53
2.6	1.2	5.1	0.55(1)	5.2(7)	.49(6)	0.92(29)	10.5(5)	.24(2)	0.65(3)	.46	.54
2.8	0.66	3.7	0.41(6)	4.0(3)	.48(4)	0.49(7)	9.3(2)	.24(2)	0.55(1)	.40	.60
3.2	0.52	2.5	0.27(1)	2.8(2)	.41(2)	0.30(2)	8.0(1)	.24(1)	0.39(1)	.32	.68
3.6	0.49	3.2	0.14(1)	2.0(2)	.38(3)	0.19(1)	7.1(1)	.22(1)	0.26(1)	.27	.73
4.0	0.46	3.2	0.26(7)	2.0(1)	.48(3)	0.15(2)	6.6(1)	.15(1)	0.20(1)	.28	.72
4.6	0.31	2.1	0.26(6)	1.3(1)	.48(3)	0.12(1)	5.7(1)	.10(1)	0.12(1)	.18	.82
5.2	0.44	3.6	0.31(17)	1.0(2)	.50(6)	0.39(13)	5.3(1)	.08(2)	0.07(1)	.15	.85
5.8	0.18	2.0	0.40(23)	0.74(25)	.50(4)	0.14(2)	4.6(1)	.08(1)	0.03(1)	.08	.92

[a] Obtained by a two-set Debye model; χ in units of 10^{-6} m^3 mol^{-1}. $R(\chi')$ and $R(\chi'')$ – discrepancy factors of the fit. Standard deviation of the last digit in parentheses.

Table S7. Temperature dependence of AC susceptibility parameters for **2** at B_{DC} = 0.40 T.

T/K	$R(\chi')$ /%	$R(\chi'')$ /%	χ_S	χ_{LF}	α_{LF}	τ_{LF} / s	χ_{HF}	α_{HF}	τ_{HF} /10^{-3} s	x_{LF}	x_{HF}
2.0	0.16	5.0	0.36(14)	1.1(4)	.00(2)	1.5(8)	10.0(4)	.25(1)	0.66(2)	.08	.92
2.2	0.93	4.2	0.59(8)	1.4(2)	.00(10)	1.1(2)	9.4(1)	.25(1)	0.60(2)	.09	.91
2.4	0.70	3.4	0.58(7)	1.4(2)	.05(8)	1.1(2)	8.8(1)	.26(1)	0.53(1)	.10	.90
2.6	0.56	2.6	0.56(6)	1.3(1)	.04(7)	0.92(11)	8.2(1)	.26(1)	0.46(1)	.10	.90
2.8	0.45	2.2	0.54(4)	1.2(1)	.09(6)	0.87(12)	7.8(1)	.25(1)	0.41(1)	.09	.91
3.2	0.26	1.9	0.56(3)	0.99(5)	.04(4)	0.64(5)	6.9(1)	.25(1)	0.32(1)	.07	.93
3.6	0.29	1.8	0.43(4)	0.90(7)	.25(6)	0.64(10)	6.2(1)	.23(1)	0.24(1)	.08	.92
4.0	0.28	2.0	0.50(4)	0.83(6)	.20(6)	0.27(3)	5.6(1)	.18(1)	0.18(1)	.06	.94
4.6	0.28	1.6	0.53(4)	0.76(6)	.32(8)	0.23(5)	5.0(1)	.12(1)	0.12(1)	.05	.95
5.2	0.11	5.7	0.29				4.3(1)	.11(2)	0.07(1)	-	1.0
5.8	0.64	5.1	0.30				3.9(1)	.09(1)	0.04(1)	-	1.0

[a] Obtained by a two-set Debye model; χ in units of 10^{-6} m^3 mol^{-1}. $R(\chi')$ and $R(\chi'')$ – discrepancy factors of the fit. Standard deviation of the last digit in parentheses.

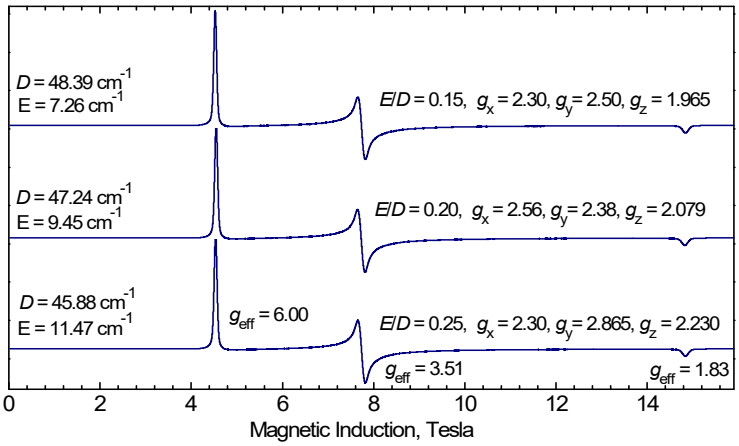

Figure S10. Different sets of the *D*, *E* and intrinsic *g* parameters result in the same effective *g* values 6.00, 3.51 and 1.83 as seen in the simulated spectra. Each pair of the *D* and *E* values produces a 100 cm^{-1} gap between the ±½ and ±3/2 Kramers doublets.

Calculation of *D*, *E* and the intrinsic g values for 2.

The anisotropy of zero-field splitting may be defined as $\eta = E/D$. Using the basic equations

$$D = D_{zz} - \frac{D_{xx} + D_{yy}}{2}$$

$$E = \frac{D_{xx} - D_{yy}}{2}$$

One can derive

$$\eta = \frac{E}{D} = \frac{(D_{xx} - D_{yy})/2}{D_{zz} - (D_{xx} + D_{yy})/2} = \frac{(D_{xx} - D_{yy})}{2D_{zz} - (D_{xx} + D_{yy})}$$

Note that reference () incorrectly defines η as

$$\eta = \frac{D_{xx} - D_{yy}}{D_{zz} - (D_{xx} + D_{yy})/2}$$

(supplementary material to Nat. Commun. 2014, 5 (1), 5300.)

We employed formulas (from Nat. Commun and Inorg. Chem. 2019) to calculate the intrinsic g_x, g_y and g_z values from the effective g components as a function of $\eta = E/D$.

$$\frac{g_{eff\,x}}{g_x} = 1 + \frac{1 - 3\eta}{\sqrt{1 + 3\eta^2}}$$

$$\frac{g_{eff\,y}}{g_y} = 1 + \frac{1 + 3\eta}{\sqrt{1 + 3\eta^2}}$$

$$\frac{g_{eff\,z}}{g_z} = \frac{2}{\sqrt{1 + 3\eta^2}} - 1$$

Since the deviations of the intrinsic g values from g of the free electron are approximately proportional to the D_{ii} tensor components, like $D_{ii} = -\lambda(g_{ii} - 2.0023)$ etc., the above equation for η can be expressed using the (intrinsic) g components:

$$\eta(g) = \frac{g_{xx} - g_{yy}}{2g_{zz} - (g_{xx} + g_{yy})}$$

The aim is to find a value of η such that the intrinsic g_{xx}, g_{yy} and g_z values calculated from formulas above would produce $\eta(g)$ equal to η. In our case, this happens for η = 0.23266, resulting in g_x = 2.381, g_y = 2.557, g_z=2.092, D=41.27 cm^{-1}, E=9.59 cm^{-1}.

However, simulation using these parameters is inaccurate (green trace in Figure S11). This probably means that the relations $D_{ii} = -\lambda(g_{ii}-2.0023)$ may not be accurate enough. A better result was obtained by fixing the intrinsic g_z value to 2.002 and fitting the resonance fields shown in Figure 6 using the spin Hamiltonian for S=3/2 while keeping the condition $2\sqrt{D^2 + 3E^2} = 89\ cm^{-1}$

In this way, a parameter set g_x= 2.316, g_y=2.473, g_z=2.002, D = 42.35 cm^{-1}, E = 7.895 cm^{-1} was obtained which resulted in better simulation (red trace in Figure S11).

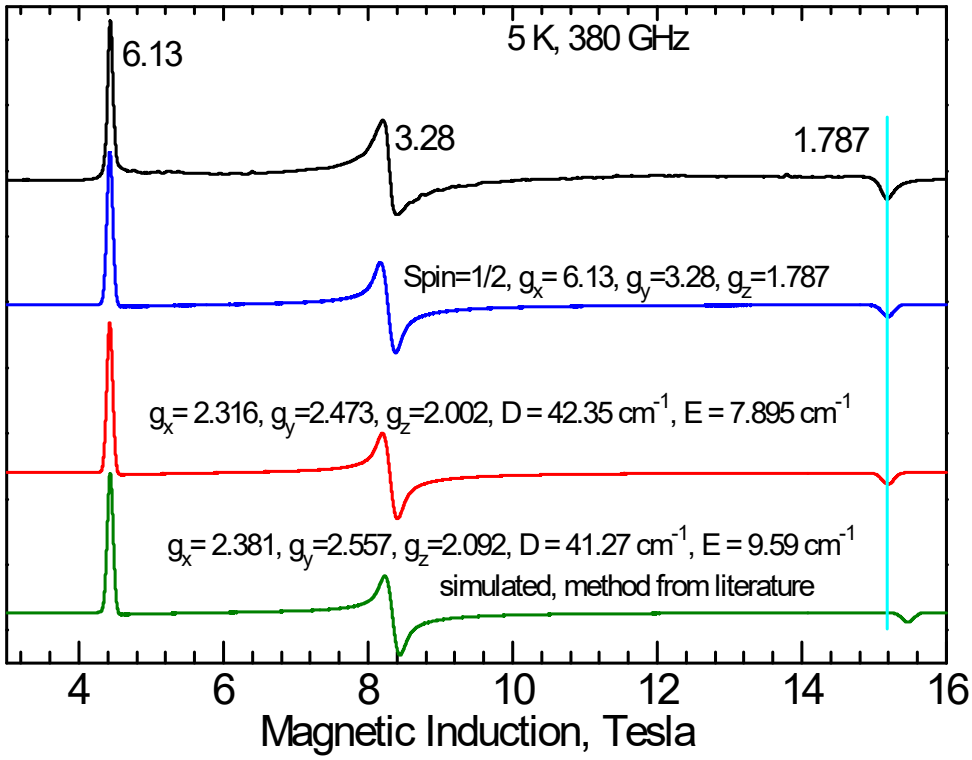

Figure S11. When the 380 GHz spectrum of **2** (black trace) is simulated using the S=3/2 parameters found above, g_x = 2.381, g_y = 2.557, g_z=2.092, D=41.27 cm^{-1}, E=9.59 cm^{-1}, the highest-field transition (g_{eff} =1.787) is simulated at somewhat incorrect position (the green trace).

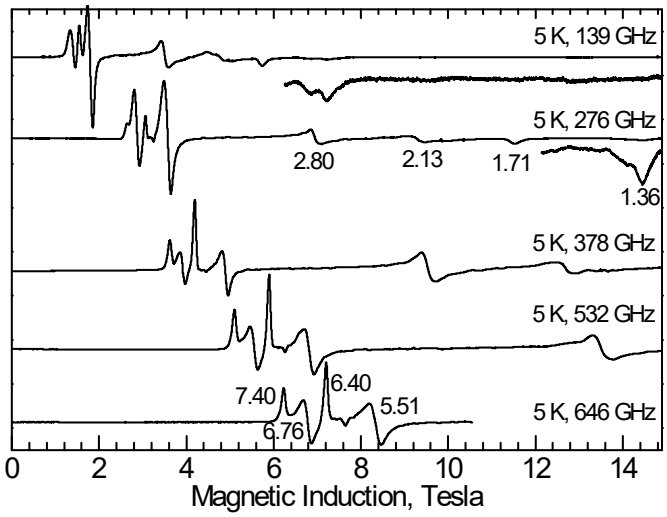

Figure S12. HFEPR spectra of **1**. The effective *g* values are shown.